Chapter 6

Structure refinement of the α-spectrin SH3 domain by means of 3D ^{15}N-^{13}C-^{13}C dipolar correlation spectroscopy and chemical shift analysis

6.1 Introduction

In the previous Chapter it was demonstrated that two dimensional spectroscopy was sufficient to obtain the typical β-sandwich fold of the small SH3 domain. For the structure calculation, 292 ^{13}C-^{13}C and ^{15}N-^{15}N restraints were derived from 2D homonuclear PDSD experiments. For investigations on larger proteins or determination of structures with higher resolution additional restraints are required. For instance, carbon-nitrogen distances could be measured with dipolar correlation spectroscopy[1-3] on selectively or uniformly ^{13}C-^{15}N-labelled samples. Alternatively, ^{1}H-^{1}H restraints could be obtained by proton-proton correlation spectroscopy, most favourable from samples deuterated at non-exchangeable sites[4,5]. In addition, angular restraints could be used in structure calculation, and recently the measurement of multiple φ torsion angles in uniformly labelled proteins was achieved from 3D ^{15}N-^{13}C-^{13}C-^{15}N dipolar-chemical shift correlation spectroscopy[6]. Three-dimensional techniques can also be used to resolve carbon-carbon correlations that could not be assigned from 2D data only, by means of ^{15}N chemical shifts. In this Chapter, 3D ^{15}N-^{13}C-^{13}C experiments are used to refine the solid-state NMR structure of the α-spectrin SH3 domain.

6.2 3D ^{15}N-^{13}C-^{13}C dipolar correlation spectroscopy

To resolve as many backbone-backbone or backbone-side-chain cross-peaks as possible, we have introduced a set of 3D ^{15}N-^{13}C-^{13}C experiments of the type NCACX and NCOCX (where “CX” stands for any carbon atom). These experiments were performed on the two

biosynthetically site-directed ^{13}C-enriched samples (see Chapter 4). In the 3D ^{15}N-^{13}C-^{13}C spectra, the improved resolution obtained by the additional ^{15}N dimension allows the identification of backbone carbon-carbon restraints of the type C^{α}-CO, CO-C^{α}, C^{α}-C^{α} and CO-CO and restraints involving side-chain carbons, which are not accessible in the 2D experiments (see Chapter 5). Due to the biosynthetically derived labelling pattern, labels are either present in the C^{α} or CO position of most of the amino-acids, while only few residues will have labels in both positions. Any of the four possible backbone carbon-carbon correlation cross-peaks involving C^{α} and CO needs therefore to be considered as a source for structure defining restraints. Since the position of the C^{β} with respect to the backbone atoms of the same amino-acid is only moderately conformationally dependent, distances of the type C^{α}-C^{β} and CO-C^{β} need to be considered as secondary structure defining distances as well, also for balancing out eventual scarcity of restraints between backbone carbons due to the lack of labels in appropriate places. Restraints between C^{α}-C^{α} and CO-CO backbone carbons occur twice in NCACX and NCOCX spectra, hence they may be resolved by two different nitrogen chemical shifts and assigned with less ambiguity; interactions which occur between a backbone carbon and side-chain carbons (e.g. between a C^{α} located in one helix and a methyl group located in another helix) occur only once in the set of spectra and can only be resolved by means of one nitrogen chemical shift.

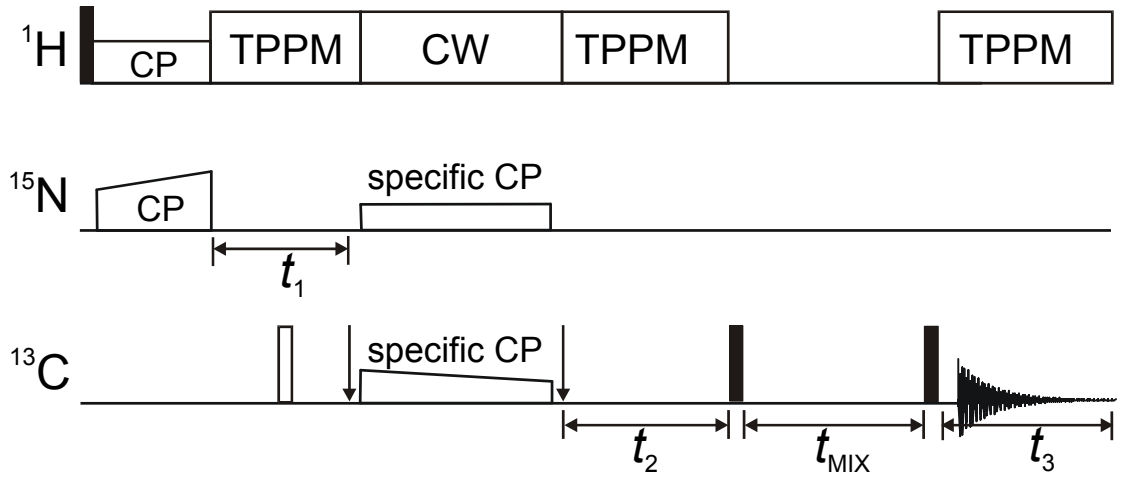

Fig. 6.1 Pulse sequence for the 3D NCACX and NCOCX experiments. The 3D ^{15}N-^{13}C-^{13}C heteronuclear dipolar correlation experiment starts with ^{1}H-^{15}N CP transfer followed by a ^{15}N evolution period. The ^{15}N magnetization is then transferred to the C^{α} or CO carbons via a specific-CP step, achieved by applying weak *rf* fields, on resonance with the ^{15}N amides in the ^{15}N channel and off-resonance in the ^{13}C channel. The vertical arrows indicate a switch in the frequency offset, required for the specific-CP. After the carbon evolution period, the carbon magnetization is exchanged using a PDSD mixing unit. During evolution and acquisition periods, a TPPM decoupling is applied, while during specific-CP continuous wave (CW) decoupling is used.

As shown in Fig. 6.1, the 3D experiments consist of an indirect ^{15}N evolution period followed by specific-CP[7], to selectively transfer magnetization from ^{15}N to $^{13}C^{\alpha}$ or from ^{15}N to ^{13}CO. In a second evolution period the ^{13}C magnetization evolves under the $^{13}C^{\alpha}$ or ^{13}CO isotropic chemical shifts and subsequently is exchanged to surrounding carbons via a PDSD mixing unit[8]. To detect inter-residue correlations, a long mixing time of 500 ms is used. In total, four different 3D experiments can be performed, combining the NCOCX and NCACX sequences with the two glycerol-made samples. However, in 2-SH3 most of the C^{α} of hydrophobic and aromatic residues are labelled and the carbonyl carbons are unlabelled, while the opposite situation is observed for 1,3-SH3. As a consequence, two of the four combinations, the NCACX experiment recorded on 2-SH3 and the NCOCX experiment recorded on 1,3-SH3, will most effectively provide the largest number of ^{13}C-^{13}C structural restraints.

6.3 3D NCACX on 2-SH3

In Fig. 6.2a, a contour plot of the 3D NCACX correlation experiment recorded on 2-SH3 is shown. Many signals are observed in the α-region (50-70 ppm) and in particular for each C^{α}-labelled residue, the intra-residue correlation $^{15}N_i$ -$^{13}C^{\alpha}_i$-$^{13}C^{\alpha}_i$ is observed as well as signals of the type $^{15}N_i$ -$^{13}C^{\alpha}_i$-$^{13}C^{\alpha}_j$, which are due to magnetization exchange between different C^{α}. In addition, signals are observed in the β- and γ-region (0-50 ppm), due to magnetization exchange between C^{α} and labelled side-chain carbons, and in the carbonyl and aromatic region (100-180 ppm, not shown), due to transfer to CO and aromatic side-chains. As an example, the assignment of the long-range correlation between K43 and F52 is illustrated in Fig. 6.2. The two long-range peaks, C^{α}_{K43} -C^{α}_{F52} and C^{α}_{F52} -C^{α}_{K43}, are not resolved in the 2D spectrum (Fig. 6.2b), but are separated in two different ^{15}N planes of the 3D NCACX spectrum. One correlation appears in the ^{15}N plane of K43 at 123.5 ppm, together with the intra-residue correlation of K43 (Fig. 6.2d), and the second long-range correlation is found in the ^{15}N plane of F52 at 118.6 ppm, together with the intra-residue correlation peak of F52 (Fig. 6.2c). Additionally, in the ^{15}N plane of K43, correlations with the aromatic C^{γ} and C^{ε} carbons of F52 are identified, while in the ^{15}N plane of F52, a correlation with C^{γ}_{K43} can be observed. Likewise, correlations between residues V44-G51 and W42-V53 could be identified from the 3D spectrum, defining, together with the correlation K43-F52, one of the anti-parallel β-sheets of the SH3 domain.

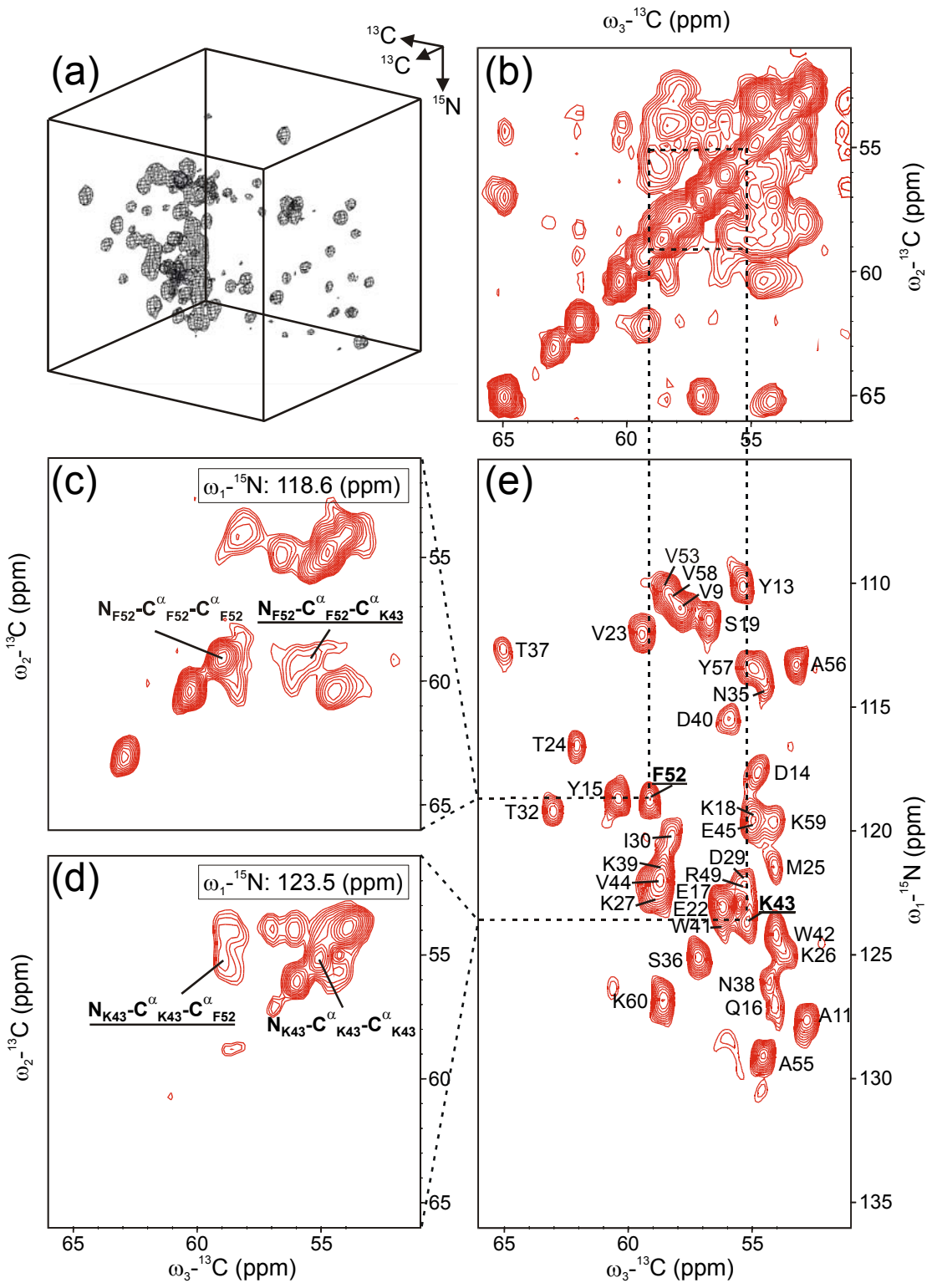

Fig. 6.2 Assignment strategy for the 3D NCACX experiment. In (a), a contour plot with a single contour of the 3D NCACX spectrum is shown. The region displayed in the plot is the aliphatic region. The spectrum was recorded on 2-SH3 sample at 9.4 T and using a spinning frequency of 8.0 kHz. In (b), the α-region of the ^{13}C-^{13}C projection of the 3D is displayed. The dotted lines indicate the positions of C^{α}_{K43}-C^{α}_{F52} and C^{α}_{F52}-C^{α}_{K43} correlations, not resolved in 2D spectroscopy. The two residues have different ^{15}N chemical shifts, as shown in the 2D NCA spectrum in (e), and in the 3D spectrum the two long-range correlations are resolved in two different ^{15}N planes, displayed in (c) and (d).

In total, 168 new inter-residue correlations could be assigned from the NCACX spectrum. From these correlations, 74 are sequential, 31 are medium-range and 63 are long-range. Since the 3D data were recorded with a single ^{13}C-^{13}C PDSD mixing time, the cross-peak intensities could not be readily translated into a distance class, hence we classified these correlations in the class with distances in the range of 2.5–7.5 Å.

6.4 3D NCOCX on 1,3-SH3

The NCOCX experiment recorded on 1,3-SH3 is shown in Fig. 6.3a. The contour plot comprises both carbonyl and aliphatic regions. In the carbonyl region, peaks of the type ($^{15}N_{i+1}$-$^{13}CO_i$-$^{13}CO_i$) are detected for all residues except leucines, that do not have a labelled CO in 1,3-SH3. In the same region correlations of the type ($^{15}N_{i+1}$-$^{13}CO_i$-$^{13}CO_j$) appear, due to magnetization exchange between carbonyl atoms of different residues. The assignment of inter-residue correlations was done by searching for pairs of peaks ($^{15}N_{i+1}$-$^{13}CO_i$-$^{13}CO_j$ and $^{15}N_{j+1}$ $^{13}CO_j$-$^{13}CO_i$) appearing in the two ^{15}N planes of residues i+1 and j+1. As an example, the assignment of the long-range correlation between K27 and Y13 is illustrated in Fig. 6.3. In the ^{15}N plane at 116.7 ppm, corresponding to the nitrogen chemical shift of G28, the diagonal-peak N_{G28}-CO_{K27}-CO_{K27} appears, together with the sequential peak N_{G28}-CO_{K27}-CO_{K26} and the long-range correlation N_{G28}-CO_{K27}-CO_{Y13} (Fig. 6.3c). At the same nitrogen chemical shift also T24 resonates, hence other peaks appear in Fig. 6.3c as well and are labelled with the respective assignments. In the ^{15}N plane of D14 at a unique chemical shift of 117.7 ppm, the diagonal peak N_{D14}-CO_{Y13}-CO_{Y13} appears, together with a sequential and two long-range correlations CO_{Y13}- CO_{K27} and CO_{Y13}- CO_{K26} (Fig. 6.3d). In the aliphatic region of the spectrum, several correlations are observed. In particular in the C^α region, correlations of the type $^{15}N_{i+1}$ ^{13}-CO_i -$^{13}C^\alpha_j$ are detected. For example, in three different ^{15}N planes of the 3D experiment, peaks could be assigned to N_{L31}-CO_{I30}-C^α_{L10}, N_{L10}-CO_{V9}-C^α_{L31}, N_{L33}-CO_{T32}-C^α_{L8}, defining one of the anti-parallel β-sheet of the SH3. Since in 1,3-SH3, the leucines have the carbonyl unlabelled and the valines the C^α unlabelled, the long-range peaks N_{A11}-CO_{L10}-C^α_{I30}, N_{T32}-CO_{L31}-C^α_{V9}, N_{L33}-CO_{L8}-C^α_{T32}, also expected because of the proximity of the two strands of the β-sheet, cannot be observed.

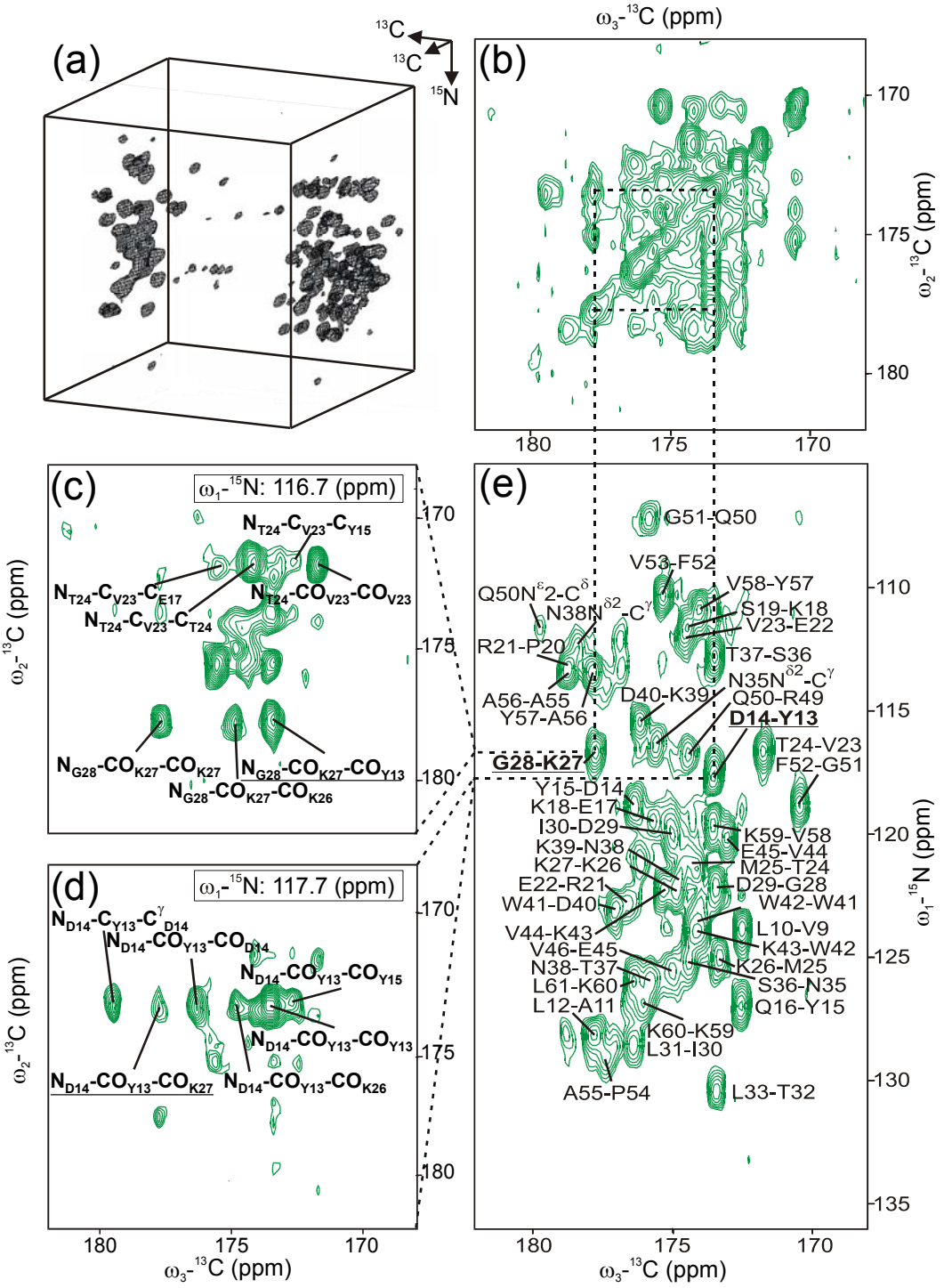

Fig. 6.3 Assignment strategy for the 3D NCOCX experiment. In (a), a contour plot with a single contour of the 3D NCOCX spectrum is shown. The plot includes the carbonyl and aliphatic regions of the spectrum. The spectrum was recorded on 1,3-SH3 sample at 9.4 T and using a spinning frequency of 8.0 kHz. In (b), the carbonyl region of the ^{13}C-^{13}C projection is displayed. The dotted lines indicate the positions of CO_{Y13}-CO_{K27} and CO_{K27}-CO_{Y13} correlations, not resolved in 2D spectroscopy. Because of the different ^{15}N chemical shifts of residues G28 and D14 in the 2D NCO spectrum in (e), the long-range correlation between K27-Y13 could be identified from the 3D NCOCX spectrum. In (c) and (d), the planes of the NCOCX at 116.7 and 117.7 ppm are displayed, with the assignment of the two peaks N_{G28}-CO_{K27}-CO_{Y13} and N_{D14}-CO_{Y13}-CO_{K27}, defining this long-range correlation.

In total, 206 new inter-residue correlations could be assigned from the 3D NCOCX dataset. From these correlations, 69 are sequential, 24 are medium-range and 115 are long-range. These correlations were classified in the class with distances in the range of 2.5–7.5 Å.

6.5 Angular restraints from chemical shift analysis

The signals observed in a MAS solid-state NMR spectrum resonate at the isotropic chemical shifts, similar to solution NMR. This has two important consequences. First of all, chemical shift databases like the BioMagnResBank, compiled from solution NMR data, can be assessed for the resonance assignment in solid-state NMR. This has been applied for the side-chain assignment of amino-acids for various proteins[9-12]. Second, the secondary chemical shift, i.e. the difference between the measured isotropic chemical shift and the corresponding random-coil value, contains information about secondary structure motifs[13-16]. In Fig. 6.4, histograms of C^{α} and C^{β} secondary chemical shift distribution in α-helical and β-sheet secondary structures are shown[17]. From the distribution of shifts it can be seen that for α-helix the average C^{α} secondary shift is around 3.1 ppm and the average C^{β} secondary shift is around –0.4 ppm, while for β-sheet $\delta_C{}^{\alpha}$= –1.5 ppm and $\delta_C{}^{\beta}$= 2.2 ppm.

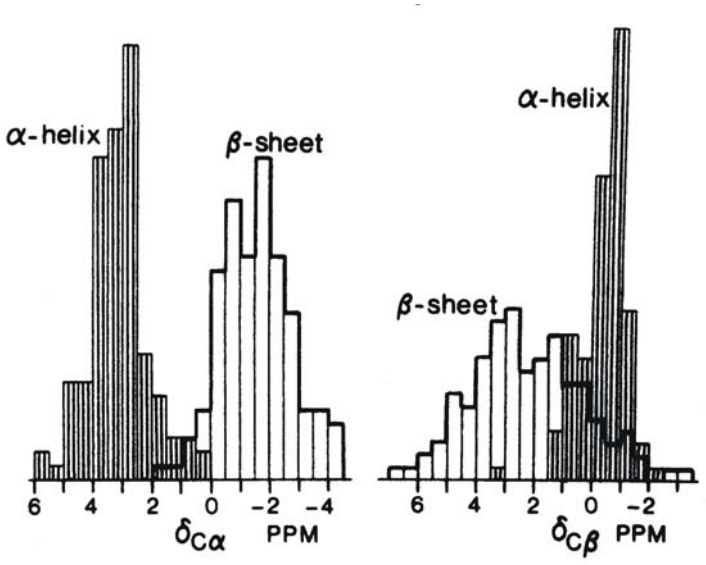

Fig. 6.4 Histograms of secondary shift distributions in α-helix and β-sheet.

Taking full advantage of the almost complete solid-state MAS NMR ^{1}H, ^{13}C and ^{15}N resonance assignments for the SH3 domain[10,18,19], an improvement of the structure can be

achieved by using the information contained in the chemical shift to obtain additional angle restraints for the structure calculation. The program TALOS[14] was used to predict backbone torsion angles, from the C^{α}, C^{β}, CO, NH and H^{α} chemical shifts of the SH3 domain. TALOS uses the secondary shifts of a given residue, together with the chemical shift information of the previous and the next one, to make prediction of the central residue. The prediction is done by comparing the secondary shifts values of each triplet of the protein with triplets in reference proteins of known structure. The TALOS database currently consists in 20 well-defined (2.2 Å or better) x-ray crystal structures, representing around 3000 triplets. TALOS searches in the database for the 10 best matches to a given triplet, and displays the values for the ϕ and ψ in a Ramachandran plot, as shown on the left side of Fig. 6.5.

Fig. 6.5 Graphical interface of the program TALOS, which summarizes the predictions for the protein backbone torsion angles. In this figure, the result obtained for residue M25 of the SH3 domain is shown., and classified as "good" prediction. On the left side of the figure, the Ramachandran plot with the 10 best database matches for the currently selected residue (M25) is displayed. On the upper-right side, the protein sequence is shown, with each residue coloured according to its classification. On the lower-right side, a list of the protein triplets, where the 10 best matches were found, is reported.

In this figure, the prediction for the residue M25 of the SH3 domain is shown. On the low-right side of the figure, the list of protein triplets where the best 10 matches are found, is shown. If the 10 matches have consistent values for ϕ and ψ, then their averages and their standard deviations are used as a good prediction. Likewise, for each residue a prediction is made and classified as "good", "ambiguous" or "bad" and represented with green, yellow and

red colours respectively, as shown in the upper-right corner of Fig. 6.5. In the case of the SH3 domain, for 29 residues (coloured in green in Fig. 6.5), ϕ and ψ backbone torsion angle predictions with sufficient reliability were made and used in the structure calculation, together with the distance restraints obtained by 2D and 3D dipolar correlation spectroscopy.

6.6 Structure calculations

We have performed two structure calculations of the α-spectrin SH3 domain. For a first calculation, only distance restraints were used. A list of 889 inter-residue restraints was generated for residues 7-61 of the SH3 domain, obtained from 2D[20] and 3D spectroscopy. A conventional structure calculation protocol with simulated annealing and torsion-angle dynamics[21] was applied and the 10 lowest-energy structures were selected. The C^{α} coordinates of the regular structure elements showed an r.m.s. deviation of 1.1 Å with respect to the average structure and of 1.6 Å to the x-ray structure[22]. In Fig. 6.6a the family of 10 structures is shown in blue, overlaid with the x-ray structure (in red)[22]. By adding the 58 dihedral-angle restraints from TALOS[14] in a second structure calculation, more refinement was achieved and the r.m.s. deviation to the average structure is reduced to 0.7 Å. This structure is also closer to the x-ray structure, with a deviation of 1.2 Å. In Fig. 6.6b, the 10 lowest-energy structures are shown in blue and superimposed on the x-ray structure (in red)[22]. The final MAS NMR structure is in general well defined. The most refined part is the β-sheet, while a lower degree of convergence is observed in the loop regions. A difference is found for residue E7. The first 6 residues of the protein are not detected in our MAS spectra, due to flexibility of the N-terminus, and are not displayed in the figure.

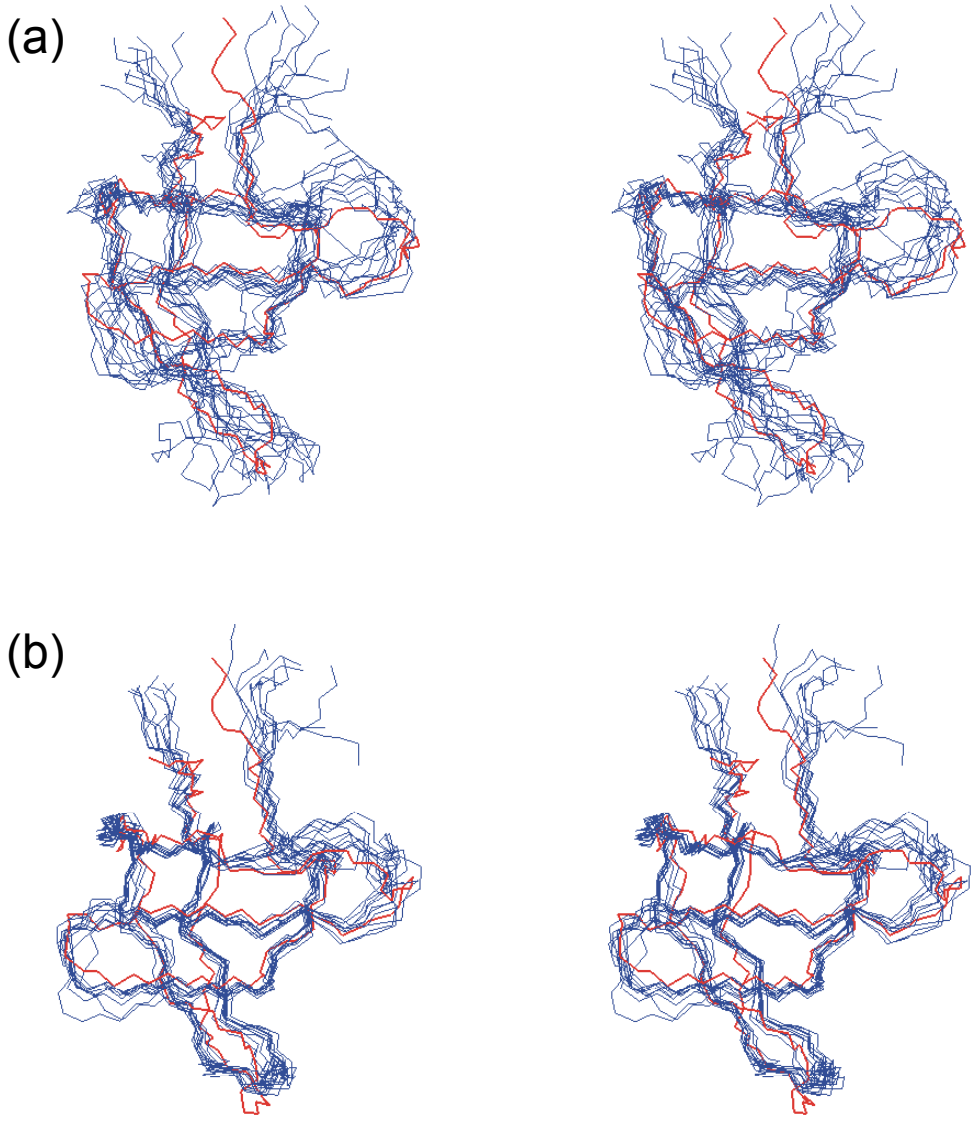

Fig. 6.6 (a), Stereo view of ten lowest-energy structures of the α-spectrin SH3 domain, coloured in blue. The structure are calculated using only distance restraints. For comparison, the x-ray structure is included, displayed in red and overlaid with the family of ten solid-state structures by fitting the backbone C^{α} atoms to the average solid-state structure. (b), Refined structures are obtained using both distance and angular restraints. In blue, stereo view of the ten lowest-energy structures, representing the fold of the α-spectrin SH3 domain, superimposed to the x-ray structure, in red.

6.7 Conclusions

Using 3D NMR spectroscopy and chemical shift analysis, a refined structure of the α-spectrin SH3 domain was obtained, exclusively derived from solid-state MAS NMR data. The fold of the SH3 domain consists of seven strands that form two orthogonal anti-parallel β-sheets. A large number of backbone carbon restraints defining the β-sheet structure could be extracted from ^{15}N-^{13}C-^{13}C dipolar correlation experiments, due to the enhanced resolution achieved by adding a ^{15}N dimension to the experiment. In particular, cross-peaks of the type C^{α}-C^{α}, CO-CO, C^{α}-CO and CO-C^{α} could be resolved, that were not possible to be extracted from 2D spectra only, because of the limited C^{α} and CO dispersion. We expect that the same methodology can be applied to probe other secondary structure motives like parallel β-sheet or helices, that are characterized by structure-defining ^{13}C-^{13}C distances in the measurable range up to ~7 Å.

6.8 Materials and methods

6.8.1 Sample preparation

The 2-SH3 and 1,3-SH3 protein samples were prepared as described in Chapter 4.4.1. Approximately 10 −12 mg of protein was used for each 3D experiment and confined to the centre of a 4 mm rotor by use of spacers.

6.8.2 Solid-state NMR spectroscopy

The 3D ^{15}N-^{13}C-^{13}C heteronuclear dipolar correlation experiments were performed on a DMX-400 spectrometer (Bruker, Karlsruhe, Germany) operating at a field of 9.4 T and equipped with a 4 mm triple-resonance CP/MAS probe (Bruker, Karlsruhe, Germany). The datasets were recorded at 280 K and at MAS frequency $\omega_R/2\pi$ = 8.0 kHz. On the ([2-^{13}C]glycerol, ^{15}N) SH3 sample an experiment of the type NCACX was performed, where the magnetization is transferred first from nitrogen to the C^{α} atoms and subsequently to the other carbons. In the 3D experiment recorded on the ([1,3-^{13}C]glycerol, ^{15}N) SH3, the magnetization transfers from ^{15}N to the carbonyl atoms and then to the other carbons. For both experiments the same pulse sequence has been applied, depicted in Fig. 6.1. Following

^{1}H excitation, a ramped cross-polarization contact of 500 μs between ^{1}H and ^{15}N created the initial ^{15}N magnetization; spin lock fields were 33 kHz for ^{1}H and 19-26 for the ^{15}N ramp. In the centre of the first ^{15}N evolution period, a π pulse on the carbon channel was applied to refocus heteronuclear ^{15}N-^{13}C scalar couplings. Following the nitrogen evolution, specific-CP[7] was employed to selectively transfer magnetization from ^{15}N to $^{13}C^{\alpha}$, in the case of ([2-^{13}C]glycerol, ^{15}N) SH3 sample, and from ^{15}N to ^{13}CO, in the case of ([1,3-^{13}C]glycerol, ^{15}N) SH3 sample. In both experiments, weak *rf* powers corresponding to nutation frequencies of ~10 kHz for the ^{15}N and ~20 kHz for the ^{13}C were used and the amide ^{15}N were irradiated close to resonance while the $^{13}C^{\alpha}$ and ^{13}CO off-resonance. The ^{13}C frequency offset was varied to match the appropriate NCA or NCO specific-CP condition. After the specific-CP, the ^{13}C carrier frequency was placed back in the aliphatic region for the NCACX experiment, and in the carbonyl region for the NCOCX experiment. After the ^{13}C evolution period, the carbon magnetization was exchanged by using a PDSD mixing scheme, with a mixing time of 500 ms[8]. During all evolution periods, proton decoupling was applied, using the two-pulse phase modulation technique (TPPM), with a pulse width of 7.3 μs and a 10° phase modulation. The 3D datasets were acquired using 1794×96×96 points and dwell times of 10 μs, 60 μs and 120 μs for f3, f2 and f1, respectively; each FID was averaged from 32 scans, using a 2.6 s recycle delay, yielding a total measurement time of ~10 days for each 3D experiment.

All the solid-state data were processed with the XWINNMR software, version 2.6 (Bruker, Karlsruhe, Germany) and subsequently analysed using the program Sparky, version 3.100 (T.D. Goddard & D.G. Kneller, University of California).

6.8.3 Structure calculations

Structures were calculated with the program CNS[21], version 1.0. Calculations were performed using the simulated annealing protocol with torsion-angle dynamics, starting with 200 randomised conformers. As described in Chapter 4, the ^{13}C-^{13}C restraints obtained from 2D spectroscopy, were classified in strong (2.5–4.5 Å), medium (2.5–5.5 Å), weak (2.5–6.5 Å) or very weak (2.5–7.5 Å). The six ^{15}N-^{15}N correlations were restrained to 3–6 Å. These data are supplemented with the 374 inter-residue ^{13}C-^{13}C restraints obtained from the 3D spectra, categorised in the "very weak" class. Prediction of torsion angles was performed using the

TALOS software[14]. In total, 58 predictions for the backbone torsion angles were obtained and included in the restraint list for the CNS calculation. The error margins for the angular restraints were set to a minimum value of 20º. The ten lowest-energy structures calculated using both distance and angular restraints showed no distance violations greater than 0.3 Å.

References

1. Rienstra, C. M., Tucker-Kellogg, L., Jaroniec, C. P., Hohwy, M., Reif, B., McMahon, M. T., Tidor, B., Lozano-Perez, T., & Griffin, R. G. (2002). De novo determination of peptide structure with solid-state magic-angle spinning NMR spectroscopy. *Proc. Natl. Acad. Sci. U. S. A.* **99**, 10260-10265.

2. Jaroniec, C. P., Filip, C., & Griffin, R. G. (2002). 3D TEDOR NMR experiments for the simultaneous measurement of multiple carbon-nitrogen distances in uniformly C-13, N-15-labeled solids. *J. Am. Chem. Soc.* **124**, 10728-10742.

3. Jaroniec, C. P., Tounge, B. A., Herzfeld, J., & Griffin, R. G. (2001). Frequency selective heteronuclear dipolar recoupling in rotating solids: accurate (13)C-(15)N distance measurements in uniformly (13)C,(15)N-labeled peptides. *J. Am. Chem. Soc.* **123**, 3507-3519.

4. Brown, S. P., Zhu, X. X., Saalwachter, K., & Spiess, H. W. (2001). An investigation of the hydrogen-bonding structure in bilirubin by 1H double-quantum magic-angle spinning solid-state NMR spectroscopy. *J. Am. Chem. Soc.* **123**, 4275-4285.

5. Reif, B., van Rossum, B. J., Castellani, F., Rehbein, K., Diehl, A., & Oschkinat, H. (2003). Characterization of (1)H-(1)H Distances in a Uniformly (2)H,(15)N-Labeled SH3 Domain by MAS Solid-State NMR Spectroscopy(section sign). *J. Am. Chem. Soc.* **125**, 1488-1489.

6. Ladizhansky, V., Jaroniec, C. P., Diehl, A., Oschkinat, H., & Griffin, R. G. (2003). Measurement of multiple psi torsion angles in uniformly 13C,15N-labeled alpha-spectrin SH3 domain using 3D 15N-13C-13C-15N MAS dipolar-chemical shift correlation spectroscopy. *J. Am. Chem. Soc.* **125**, 6827-6833.

7. Baldus, M., Petkova, A. T., Herzfeld, J., & Griffin, R. G. (1998). Cross polarization in the tilted frame: assignment and spectral simplification in heteronuclear spin systems. *Mol. Phys.* **95**, 1197-1207.

8. Szeverenyi, N. M., Sullivan, M. J., & Maciel, G. E. (1982). Observation of Spin Exchange by Two-Dimensional Fourier-Transform C-13 Cross Polarization-Magic-Angle Spinning. *J. Magn. Reson.* **47**, 462-475.

9. McDermott, A., Polenova, T., Bockmann, A., Zilm, K. W., Paulson, E. K., Martin, R. W., Montelione, G. T., & Paulsen, E. K. (2000). Partial NMR assignments for uniformly (13C, 15N)-enriched BPTI in the solid state. *J. Biomol. NMR* **16**, 209-219.

10. Pauli, J., Baldus, M., van Rossum, B., de Groot, H., & Oschkinat, H. (2001). Backbone and side-chain C-13 and N-15 signal assignments of the alpha-spectrin SH3 domain by magic angle spinning solid-state NMR at 17.6 tesla. *Chembiochem* **2**, 272-281.

11. Egorova-Zachernyuk, T. A., Hollander, J., Fraser, N., Gast, P., Hoff, A. J., Cogdell, R., de Groot, H. J., & Baldus, M. (2001). Heteronuclear 2D-correlations in a uniformly [13C, 15N] labeled membrane-protein complex at ultra-high magnetic fields. *J. Biomol. NMR* **19**, 243-253.

12. Hong, M. (1999). Resonance assignment of 13C/15N labeled solid proteins by two- and three-dimensional magic-angle-spinning NMR. *J. Biomol. NMR* **15**, 1-14.

13. Laws, D. D., Bitter, H. M., Liu, K., Ball, H. L., Kaneko, K., Wille, H., Cohen, F. E., Prusiner, S. B., Pines, A., & Wemmer, D. E. (2001). Solid-state NMR studies of the secondary structure of a mutant prion protein fragment of 55 residues that induces neurodegeneration. *Proc. Natl. Acad. Sci. U. S. A* **98**, 11686-11690.

14. Cornilescu, G., Delaglio, F., & Bax, A. (1999). Protein backbone angle restraints from searching a database for chemical shift and sequence homology. *J. Biomol. NMR* **13**, 289-302.

15. Jaroniec, C. P., MacPhee, C. E., Astrof, N. S., Dobson, C. M., & Griffin, R. G. (2002). Molecular conformation of a peptide fragment of transthyretin in an amyloid fibril. *Proc. Natl. Acad. Sci. U. S. A* **99**, 16748-16753.

16. Luca, S., Filippov, D. V., van Boom, J. H., Oschkinat, H., de Groot, H. J., & Baldus, M. (2001). Secondary chemical shifts in immobilized peptides and proteins: a qualitative basis for structure refinement under magic angle spinning. *J. Biomol. NMR* **20**, 325-331.

17. Spera, S. & Bax, A. (1991). Empirical Correlation Between Protein Backbone Conformation and C-Alpha and C-Beta C-13 Nuclear-Magnetic-Resonance Chemical-Shifts. *J. Am. Chem. Soc.* **113**, 5490-5492.

18. van Rossum, B. J., Castellani, F., Rehbein, K., Pauli, J., & Oschkinat, H. (2001). Assignment of the nonexchanging protons of the alpha-spectrin SH3 domain by two- and three-dimensional H-1-C-13 solid-state magic-angle spinning NMR and comparison of solution and solid-state proton chemical shifts. *Chembiochem* **2**, 906-914.

19. van Rossum, B. J., Castellani, F., Pauli, J., Rehbein, K., Hollander, J., de Groot, H. J., & Oschkinat, H. (2003). Assignment of amide proton signals by combined evaluation of HN, NN and HNCA MAS-NMR correlation spectra. *J. Biomol. NMR* **25**, 217-223.

20. Castellani, F., van Rossum, B., Diehl, A., Schubert, M., Rehbein, K., & Oschkinat, H. (2002). Structure of a protein determined by solid-state magic-angle-spinning NMR spectroscopy. *Nature* **420**, 98-102.

21. Brunger, A. T., Adams, P. D., Clore, G. M., DeLano, W. L., Gros, P., Grosse-Kunstleve, R. W., Jiang, J. S., Kuszewski, J., Nilges, M., Pannu, N. S., Read, R. J., Rice, L. M., Simonson, T., & Warren, G. L. (1998). Crystallography & NMR system: A new software suite for macromolecular structure determination. *Acta Crystallogr. D. Biol. Crystallogr.* **54 (Pt 5)**, 905-921.

22. Musacchio, A., Noble, M., Pauptit, R., Wierenga, R., & Saraste, M. (1992). Crystal structure of a Src-homology 3 (SH3) domain. *Nature* **359**, 851-855.